Structural and mechanical properties of different types of graphite used in nuclear applications

L. Kurpaska[1)], M. Frelek-Kozak[1)], M. Wilczopolska[1)], W. Bonicki[1)], R. Diduszko[2)], A. Zaborowska[1)], E. Wyszkowska[1)], M. Clozel[1)], A. Kosinska[1)], I. Cieslik[1)], M. Duchna[1)], I. Jozwik[1,2)], W. Chmurzynski[1)], G. Olszewski[1)], B. Zajac[1)], J. Jagielski[1,2)]

[1]National Center for Nuclear Research, st. A. Soltana 7, 05-400 Otwock-Swierk, Poland
[2]Institute of Electronic Materials Technology, st. Wólczynska 133, 01-919 Warsaw, Poland
corresponding author: lukasz.kurpaska@ncbj.gov.pl

Pre-print version

Abstract:

Graphite is known as a material with excellent thermo-mechanical, structural and neutron moderation properties. It is currently used as a core structural component for High Temperature Gas Cooled Reactor (HTGR). It is due to the fact that graphite has been extensively tested and proved to satisfy most of HTGR operating requirements. However, one question still remain unclear. Graphite, depending from the manufacture method, type and purity shows different mechanical and structural properties. In addition to that, literature data is poor in comparative studies of current and used in the past materials. For this reason, series of tests involving Scanning Electron Microscopy, Raman Spectroscopy, X-ray diffraction and nanoindentation have been performed on the virgin samples of two types of nuclear graphite's: IG-110 and nuclear graphite used in decommissioned EWA reactor. Obtained results clearly shows differences in microstructural and mechanical properties of both types of graphite's. Reported changes have been discusses and attributed to the density of the material and its origin.

Keywords: nuclear graphite, Raman spectroscopy, X-ray diffraction, SEM, nanoindentation

1. Introduction

Graphite has been used as a neutron moderator or reflector in nuclear applications for a very long time [1-3]. Currently, this material is proposed to be a core structural element for two types of Generation IV nuclear reactors: HTR – High Temperature Reactor, and MSR – Molten Salt Reactor [4, 5]. Usually, nuclear graphite is manufactured to contain large crystallites which are arranged randomly. Such a configuration results in isotropic macroscopic properties. Graphite crystals are anisotropic: carbon atoms are arranged in a hexagonal lattice with a strong sp2 hybridized bond in the basal plane. Basal planes are bonded by weak Van der Walls forces in the direction perpendicular to the basal plane (along the c axis).

Graphite is very resistant to radiation and maintains its favorable mechanical and structural properties in the radiation field. This is particularly important as this material has to sustain large neutron fluxes over long exposure times. The irradiation and temperature effects in nuclear graphite

have been studied for decades already [6-10]. For example, it has been proved that graphite crystallites undergo an expansion along the c axis and a shrinkage in the basal plane upon irradiation [11, 12]. Graphite, when neutron irradiated, presents a large number of point defects whose clusters are generated into the lattice structure. The reported radiation defects are accompanied with basal plane destruction, dimensional change, swelling and amorphization which is induced locally by irradiation. Depending on the dose and graphite grade, a large number of dislocations are created by formation and aggregation of vacancies and interstitials [13]. If the material is irradiated to a high dose, point defects accumulate and induce so called 'buckling' and 'ruck and tuck' defects by cross-linking between point defects on the basal layers. These defects multiply quickly and form extended defects [14]. Consequently, graphite exhibits asymmetric dimensional change which leads to the formation of complex layer defects and conclusively modifies the bonding characteristics between carbon atoms. In conclusion, the physical consequences of neutron irradiation are the disordering of basal layers and C-C bonding modification of carbon hexagonal rings in the lattice.

In order to simulate the generation of radiation defects, ion irradiation can be employed. The goal of this paper is to study the material in the pristine state, however we are planning to conduct analysis of ion irradiated samples too. For this reason, basic explanation of at least historical data seems to be appropriate. In case of graphite, noble gases like Ar, He, Xe or Kr are typically used to simulate neutron damage [15-18]. Ion irradiation can be performed using single ion beam, however, some data describing double ion irradiation can be found in the literature. It is also possible to use heavy ions, like Ne, Cr, Ni, Zn or U. The main differences between ion and neutron irradiation are: (i) larger size of the colliding particle compared to neutrons and (ii) the presence of a charge (neutrons have no charge) and the energy level (ions have energies from a few keV to a few MeV maximum, while neutrons reach energies up to 10 MeV in a fission system, and 14 MeV in a fusion one). Despite, these controversies, many researchers use ions as surrogate of neutrons as the damage created in the material imitates well the damage generated by neutrons.

The nuclear grade graphite has a polycrystalline structure which is rich in pores and cracks (porosity usually around 20%) that can accommodate irradiation induced expansion along the c axis. In general it has been proved that macroscopic dimensions of nuclear graphite undergo 3-4% shrinkage and then increase during high temperature irradiation (at 300 – 700 ^{o}C) [18]. The reported effect is related to the porosity which consists of two domains: lenticular cracks which can be from a few nm to a few µm long (including open and closed Mrozowski cracks) and more bulbous porosity. Taking into account these two porosity types, it has been proved that irradiation results in expansion of the crystallites and a closure of lenticular porosity which affects the coefficient of thermal expansion and material dimension. At the same time, bulbous porosity submitted to irradiation affects the Young modulus, thermal conductivity and material strength [19]. Despite the fact that these phenomena are quite well explained, many questions related to the microstructure, its relation with the fabrication method and finally, its impact on mechanical properties, remain unanswered. In addition to that, a significant lack of data on the nuclear graphite used in previous nuclear reactors can be seen.

In this work, Scanning Electron Microscopy (SEM), Raman Spectroscopy, X-ray Diffraction analysis were applied to study structural properties of the materials. These techniques are frequently used to study different materials, and they proved their usability in evaluating types of structural features [20, 21]. Mechanical properties like hardness or Young modulus were obtained by using nanoindentation technique. The goal of this study was to compare mechanical and structural features of two independent nuclear graphites, of which: IG-110 is planned to be used in next generation nuclear reactors (for example High Temperature Reactor) and NCBJ graphite which was previously used in

Pre-print version

decommissioned EWA research reactor located at National Center for Nuclear Research, Poland. Finally, the presented analysis serves to build competences in the field of high temperature materials. It is expected that in the future, impact of ion implantation (i.e. development of radiation defects) on the structural and mechanical features of both materials will be tested and their structural and mechanical properties at high temperature will be reported.

2. Experimental methodology

2.1. Material and sample preparation

Nuclear grade graphite IG-110, commercially manufactured by Toyo Tanso (Japan) and nuclear grade graphite used in the decommissioned EWA reactor located at National Center for Nuclear Materials, Poland, were selected for analysis. IG-110 is a fine-grained material, manufactured by isostatic pressing. The source coke is petroleum. Average grain size is 20 µm, density 1.71 g/cm^3, ash content <10 wppm and porosity ≈22%. The graphite from NCBJ is a material which was used to build critical testing assemblies and the EWA research reactor in the 1970s. The history of the material production is not available. Conducted measurements showed that the density of NCBJ nuclear graphite is 1.62 g/cm^3 while the porosity is maintained at the level of ≈28%. Samples of both materials were cut to 10 x 10 x 5 mm plates. The polishing process was conducted carefully to maintain the original microstructural features such as pore shape and surface morphology. It is known that graphite is a soft and porous material. Therefore, one must avoid contamination of the surface during polishing with the diamond paste products. EDS analysis after polishing did not reveal significant contamination like Si, Al or Na.

2.2. SEM and optical microscope

Scanning Electron Microscopy (SEM) was carried out to characterize the graphite microstructure, pores and discontinuities. Studies were performed at the microscale. In order to show the morphology of the samples, images with magnifications of: 50x, 500x and 5000x were taken. The described tests were carried out on the Scanning Electron Microscopy (SEM) provided by Zeiss EVO MA 10. The device was equipped with a Secondary Electron (SE) Bruker AXS D8 detector and special design of lens providing separation of SE and BSE signals in the real time. The electron energy used during the microstructural observations was in the range of 20 keV.

2.3. Raman spectroscopy

Raman spectra were recorded using a WiTec alpha300 R Confocal Raman microscope operated with a 532 nm laser. The samples were analyzed through a 50 µm confocal pinhole at optical magnification of 100x. One exposure per spectrum was recorded during 30 s. The penetration depth of laser light used in Raman was calculated using the formula of penetration depth = $(\alpha)^{-1}$, where α is the absorption coefficient at the given wavelength. For 532 nm Raman laser light, the penetration depth was estimated to be ≈5 µm The data was recorded at two arbitrary points on the surface of each sample. The normalized raw Raman spectra were fitted using WiTec software. Lorentz functions were used for peak fitting.

Raman spectroscopy is an important technique to characterize the microstructure of nuclear graphite materials. Especially the analysis of structural defects and in-plane crystallite size can be done by using this technique. It is known that the intensity of the defect induced D band (located ≈1350 cm$^-$

Pre-print version

[1]) compared with the Raman allowed E_{2g} mode (which is also called G band and corresponds to prominent feature of graphite material, located ≈1580 cm^{-1}) depends on the size of crystals. The in-plane crystallite size of nuclear graphite specimens IG-110 and NCBJ were calculated based on the following eq. [22, 23]:

$$L_a = 2.4 \cdot 10^{-10} \lambda_{laser}^4 \left(\frac{I_D}{I_G}\right)^{-1} \text{[nm]} \quad (1)$$

where λ_{laser} = 532 nm and I_D and I_G are intensities of I and G bands, respectively.

2.4. X-ray diffraction

In the microstructural characterization of nuclear graphite materials, XRD is a highly effective tool to determine the crystal structure and structural parameters. Therefore, the XRD patterns of the graphite specimens were performed by using a Rigaku SmartLab 3kW X-ray diffractometer with theta/theta vertical goniometer, using filtered radiation Kα1 of Cu tube, U = 40kV, I = 30 mA with an average wavelength λ = 1.5418 Å and in the Bragg-Brentano (BB) geometry was used. A 1D line detector, Dtex-Ultra250 was used. Samples were mounted to Si low backgrounds holders. Measurements were carried out with step of 2θ = 0,01° in the angular range 10-90° (2θ) at scanning speed of 1°/min. The obtained data was analyzed with use of ICDD PDF4+ (2019) data base.

2.5. Nanoindentation

In order to estimate nanomechanical properties of the graphite specimens, nanoindentation technique was employed. Nanomechanical properties (nanohardness, Young modulus) were investigated using a NanoTest Vantage® system provided by Micro Materials Laboratory. A Berkovitch-shaped diamond indenter was used for all nanomechanical measurements. Each experiment was repeated 20 times, in a line scan mode with 50 µm distance between the indents. The indents were made using 50 and 300 mN loads, which correspond to approximately 3.2 and ≈10 µm of maximal indentation depth. Measurements were performed with 15 s loading time, 5 s dwell period and 10 s total unloading time. The load/unload curves recorded in nanohardness measurements were fitted using the well-known Oliver-Pharr method. According to the Oliver-Pharr approach, the unloading curve was used for nanomechanical properties calculation [24]. One should remember that the nanoindentation method produces the reduced Young modulus (Er) values, and herein presented Young modulus of the material (E) is obtained by implementing eq. (2):

$$\frac{1}{E_r} = \frac{(1-\nu^2)}{E} + \frac{(1-\nu_i^2}{E_i} \quad (2)$$

where E_i and ν_i are the Young modulus and the Poisson's ratio of the indenter, respectively 1140 GPa and 0.07. In this study, the sample's Poisson ratio was set as 0.31 [25]. The goal of this investigation was to compare (at least qualitatively) the mechanical response of both materials and correlate it with their structural features.

Pre-print version

3. Results and discussion

Tab. 1 shows the SEM images of the polished nuclear graphites, IG-110 and NCBJ. Images were made with magnifications 50, 500 and 5000x. Bulbous pores, filler particles, binder phase or lenticular porosity were marked on both materials. One can clearly see differences in the microstructure between both materials. In all scales, IG-110 seems to be smoother and less flaky compared to the graphite from NCBJ. In general, the recorded images illustrate the heterogeneity of the materials. Large amounts of pores, grains and flakes can be found in both samples. However, one can clearly see that this phenomenon is particularly important for the graphite from NCBJ, as IG-110 shows much more compact structure (at least in this measurement scale). Large pores (of the order of several microns length, marked as lenticular porosity), uniformly distributed in the whole specimen can be observed in the NCBJ nuclear graphite. It is expected that these structural features will affect the mechanical properties of the material and will be visible on the Raman spectra and X-ray patterns, as these techniques are quite sensitive to such microstructural features. The conducted calculations suggest that Raman penetration depth will be of the order of single microns.

In this study, we did not perform any TEM investigation. However, one can use existing literature data. For example, number of studies have been performed on IG110 graphite [6]. It is commonly accepted that Mrozowski cracks and nano-cracks (which are observable at high magnification SEM) are important in the understanding of the dimensional instability of nuclear graphite at pristine state and under irradiation as they are identifiable as accommodation porosity. In general, one may expect that many cracks and pores of various sizes are formed in graphite materials during manufacture process, yet some can be formed prior to carbonization and graphitization. It is also accepted that crack growth property determines performance of nuclear graphite. For example, Kakui et al. [26], investigated crack extension under cyclic loading conditions. They proved that the paths of the cracks in graphite are closely relevant to coke grain size and cracks can preferable extend along the coke grain boundaries. It has been reported that Mrozowski microcracks are observed in crystallized graphite. Nano-cracks are observed in pseudo-crystallized binders. In addition to that, type of z-shape bending of the basal plane and delamination cracks are also observed in graphite crystallites. These cracks were formed during manufacturing process, and can be responsible for accommodation of fission products.

The implementation of TEM gives deeper insight into the material microstructure. Usually, different features like filler particles, microcracks, binder phases, quinolone insoluble (QI) particles, chaotic structures and turbostratic graphite phases may be identified. In addition to that, TEM data provides information about misorientation of the basal planes, nano-sized delamination cracks and disclinations. Finally, by using TEM one can estimate d-spacing and compare it with XRD, and report structural defects like vacancies in the basal plane (who may effect calculated d-spacing value).

Pre-print version

Tab. 1. SEM images of nuclear grade IG-100 and NCBJ graphite obtained at 50, 500 and 5000x magnification.

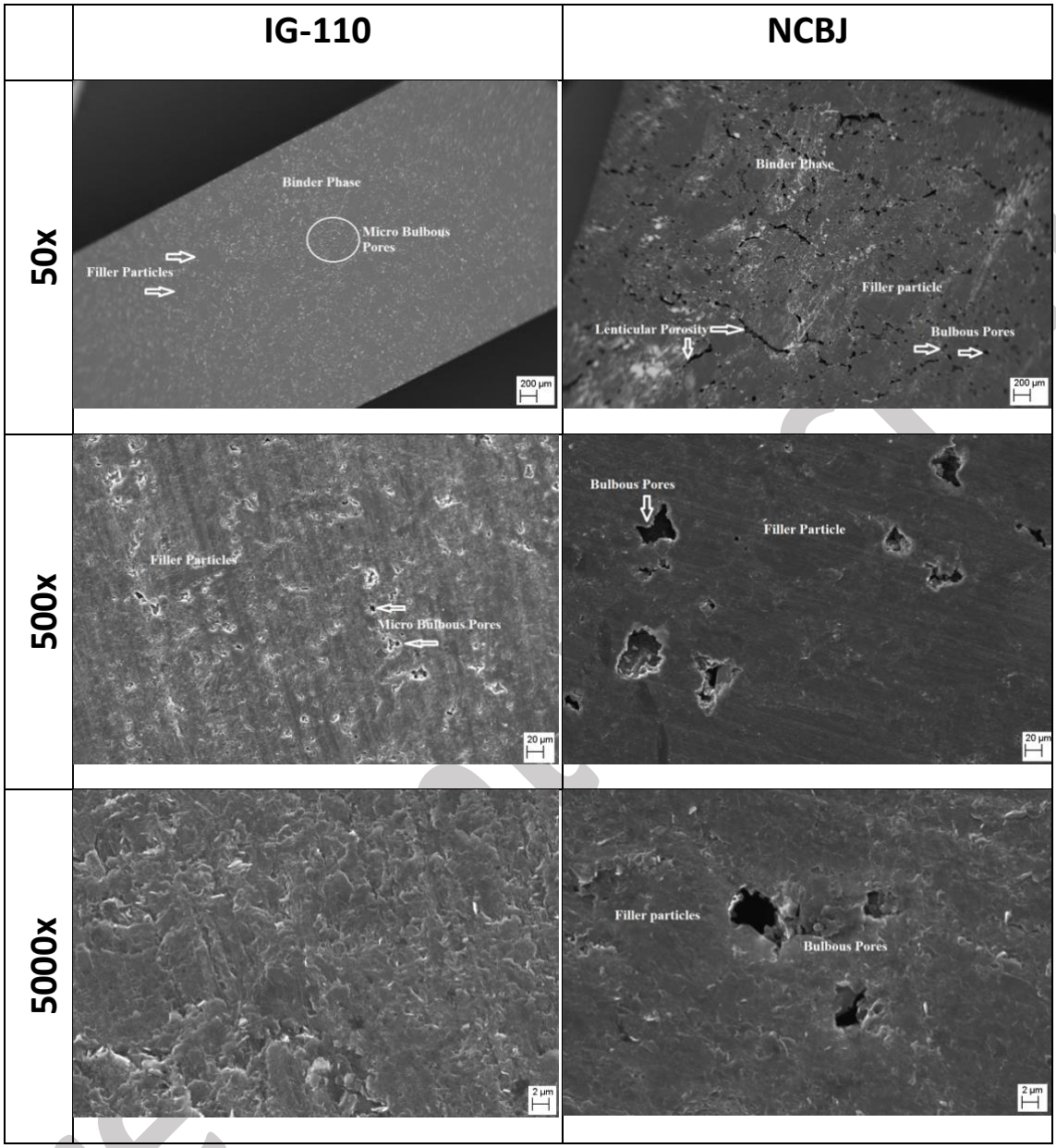

Fig. 1 shows the recorded Raman spectra of IG-110 and NCBJ nuclear graphite materials. Each analysis was performed 3 times and an average result is presented. For clarity, the fitting of the Raman bands is not shown. However, the fitting was made using the Lorenz function in the Witec software. Each material is characterized by 3 main bands: D, G and G'. The reported bands are typical for graphite materials and their presence and dependencies were reported by several authors already [28-32]. On the side of each band, its characteristic position is marked. As expected from the SEM analysis, additional low intensity bands like: D+D' or D+D'' (located on both sides of the G' band) can be observed in both materials. According to previous studies of Seehra et al. [33], these bands appear when defect content in the structure is significant. One can observe that this is a case for both specimens and this suggests the presence of defects, stacking faults and poor crystallinity. Tab. 2 summarizes the detailed interpretation of the main Raman bands present in ideal graphite. It is known

that the basal facet of an ideal, defect-free graphite contains two sharp Raman bands: G and second order G' located near 1580 and 2700 cm^{-1}, respectively. The presence of the D bands confirms the presence of defected (non-uniform) structure in the material.

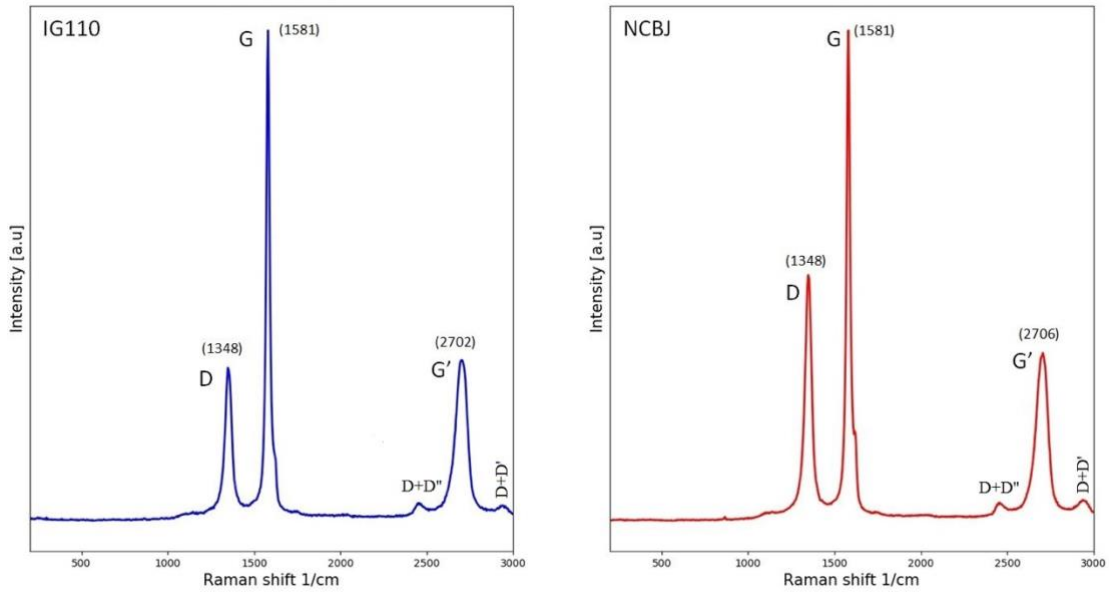

Fig. 1. Raman spectra from nuclear graphite samples, A) IG-110 and B) NCBJ. Marked on the figures Raman bands depict first order D, G and G' bands and their positions.

Tab.2. Assignment and interpretation of the Raman bands recorded in graphite material [19, 34, 35].

Raman band	Raman order	Wavenumber (cm^{-1})	Phonon modes	Corresponding graphite structure
G	First	≈1580	Doubly degenerate phonon mode with E_{2g} symmetry from sp2 carbon networks in the Brillouin zone	Present in perfect graphite, and in all graphite materials with crystallite structure. FWHM (G) increases with disorder, as well as with sp^2 content
D	First	≈1350	Non-degenerate A1' phonon arising in the vicinity of the K point at the edge of Brillouin zone. A defect is required for the activation of the mode.	Required defect for its activation, like edges which are extended defects. Also present in turbostratic materials where the interaction with adjacent layers is very week. FWHM (D) indicates broader distribution of crystallite sizes and orientations in A3
G'	First	≈2700	Overtone of the D band. A_1' phonon arising in the vicinity of the K point at the edge of the Brillouin zone. A defect is required for activation of this mode	Located near bands with low intensity (G'_2D or G'_3D) may suggest: turbostratic graphite where the interaction between adjacent layers is very weak or crystallite graphite structure

Pre-print

D+D’	Second	≈2950	Phonon density of state maximum for the LO (longitudinal acoustic mode) branch (dispersion of phonon mode)	FWHM (D+D’) increases with defect content
D+D’’	Second	≈2450	Emission of one intravalley phonon and one intervalley phonon	-

Tab. 3 summarizes the intensity and crystallite size calculated based on the eq. 1. One can observe that the D band intensity of the NCBJ graphite is much higher (almost 3x) than IG-110. This effect suggests a larger amount of defects such as large pores and edges in this material, in comparison to IG-110. Finally, the recorded intensity of D and G bands allows one to estimate the crystallite size of the specimen. The conducted calculations, which were repeated three times, show that IG-110 is characterized by bigger crystallite sizes (53.2 ± 3.2) than NCBJ graphite (38.2 ± 3.9). Actually, the literature data is not clear about the crystallite size evaluation. For example Zheng et al. [6] reported that the crystallite size of IG-110 varies between 30 to almost 45 nm, and strongly depends from the measurement position. Similar results were obtained by Wu et al. [19]. At the same time, crystallite size obtained for NCBJ graphite is similar to A-3 and NBR-18 nuclear graphite types [6, 19]. Further analysis is required to answer these questions. Especially, calculations taking into account multipoint measurements should be done to obtain better result statistics .

Tab. 3. Measured intensities of D and G bands of IG-110 and NCBJ nuclear graphite samples. Using formula (1), the crystallite size for each specimen was calculated.

	Intensity D (cm-1)	Intensity G (cm-1)	La (nm)
IG110	*4756*	*13507*	*54.6*
	2937	*8454*	*55.4*
	3991	*10282*	*49.5*
NCBJ	*12323*	*23704*	*37*
	7075	*12903*	*35.1*
	7841	*17369*	*42.6*

Fig. 2 presents XRD diffraction patterns of the two nuclear graphites: IG-110 and NCBJ. Peak indexes originating from hexagonal graphite have been marked on the diffractograms. It is characteristic that the peaks associated with crystallographic planes parallel to hexagonal graphite planes (type (00l)) and perpendicular to them (type (100) and (110)) are clear and narrow. At the same time peaks originating from the oblique planes, i.e. with indexes of (hkl) type are wide and fuzzy. This shows that the crystal structure of the studied nuclear graphite specimens is not ideal: the hexagonal planes are slightly shifted and / or twisted relative to each other, compared to the structure of the ideal graphite crystal. The reported phenomena suggest that the investigated structure of the material is at least partly turbostratic.

Pre-print version

Finally, one should keep in mind that the tests were carried out at room temperature using the same measurement conditions. The obtained results clearly indicate that the NCBJ graphite is less ordered in comparison to the IG-110 material - this particularly applies to the mutual ordering of hexagonal planes, as evidenced by greater blurring of oblique reflections, i.e. (hkl) and (h0l), (0kl). In conclusion, the diffraction patterns of both samples look similar: the type 00l, h00 and hh0 reflections are relatively narrow, while the others, type hkl - wide. This proves the "turbostratic" structure - packets of hexagonal layers, but with a weaker three-dimensional order. Parameters determined from the diffraction patterns are shown in the table (L_c i L_a were obtained using Scherrer formula):

Tab. 4. Measured interplanar distance and average thickenss of the layer packet and diameter of the hexagonal layers in IG-110 and NCBJ graphite materials.

sample	interplanar distance d_{002} [Å]	average thickness of the packet of layers L_c [Å]	average diameter of the hexagonal layers L_a [Å]
IG110	3.3640	380	700
NCBJ	3.3629	300	480

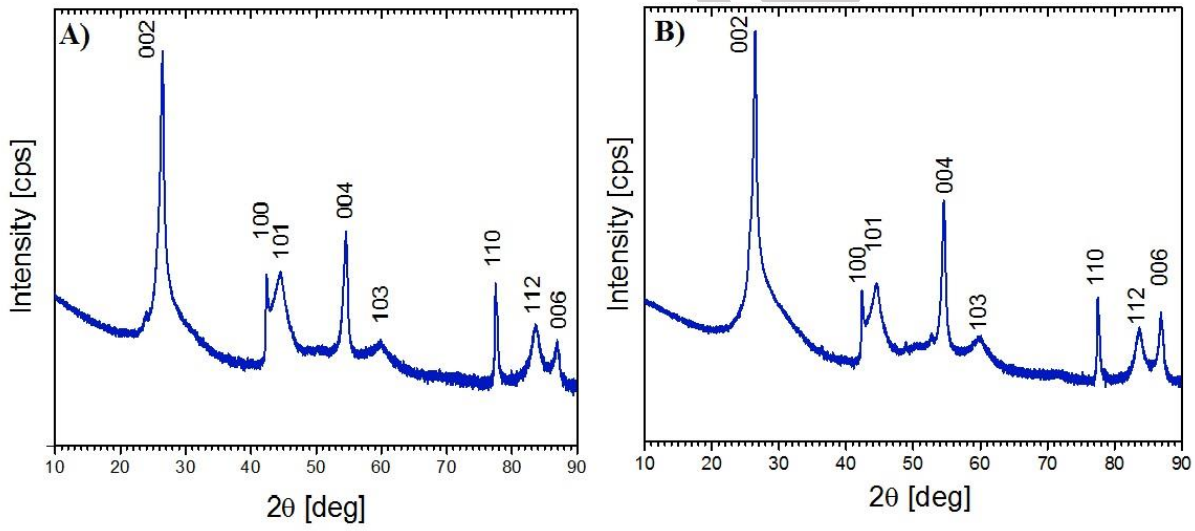

Fig. 2. XRD patterns of nuclear graphite materials A) IG-110 and B) NCBJ, 2θ range from 10 to 90°.

In order to investigate the mechanical properties of the material, nanoindentation technique was employed. Fig. 3 shows Load-Displacement curves (L-D) recorded on both materials under 50 and 300 mN loads, respectively A) and B). One can see that in the low load regime, the recorded signal from NCBJ nuclear graphite is highly scattered. This phenomena suggest that the surface of the material may not be uniform, and some discontinuities like pores, grain boundaries or edges exist in the structure. The microstructural investigations revealed the presence of the typical Mrozowski cracks and nano/micro cracks in the investigated specimens. More structural features were observed in the case of NCBJ graphite. All these features create microstructural discontinuity, which explains why the signal recorded at lower load is clearly more scattered (this is particularly visible for the NCBJ graphite). Opposite situation takes place for the measurement conducted under 300 mN load. L-D signals from both materials are clearly separated. Some scattering still exists, yet it remains at a reasonable level.

Pre version

The reduction of the scattering is most likely related to the indentation depth. Indenting specimens to 10 microns results in minimizing the impact of Indentation Size Effect (ISE) which plays a big role in small depth measurements. It is also expected that nano-sized microstructural features like pores, cracks and discontinuities will be accommodated by larger structural defects, therefore their movement doesn't play as major a role as in the case of low load tests.

Fig. 4 presents Hardness A) and Young modulus B) values of both materials measured under 50 and 300 mN loads. The goal of this investigation was to check whether indentation load (and therefore depth) impacts the recorded data. One can see similar trends for both materials: hardness and Young modulus tend to decrease with increasing load, and the recorded error bars are reduced. The values of Hardness and Young modulus quantitively and qualitatively agree with the literature data. For example, Oku et al. [10] tested several different nuclear graphite materials (IG-430U, IG-430UHP, PD-330S) and reported that Young modulus is in the range of approx. 6 to 10 GPa. One should remember that these materials had slightly higher density, approx.. 1.8-1.9 g/cm^3. Hence, this may increase recorded values.

Regarding the properties of the material submitted to irradiation, one can expect an increase in hardness due to accumulation of radiation defects. For example, Oku et al. [10] conducted 175 keV Ar-ion irradiation up to 6.2x10^12 ions/cm2. Afterwards, he measured hardness, young modulus, compressive and bending strength from the L-D data. Experiments have been performed for 6 different nuclear graphite materials and in almost all cases, an increase in all 4 parameters was recorded (except for the hardness of IG-430UHP and PD-330S). It has been showed that microhardness measurements can be used to evaluate mechanical properties of the ion-irradiated graphite. Despite this obvious point, work of Oku et al. [10] is one of the few available sources in the literature. It is expected that in the future, this group will perform similar investigations on the materials submitted to Ar and He irradiation processes.

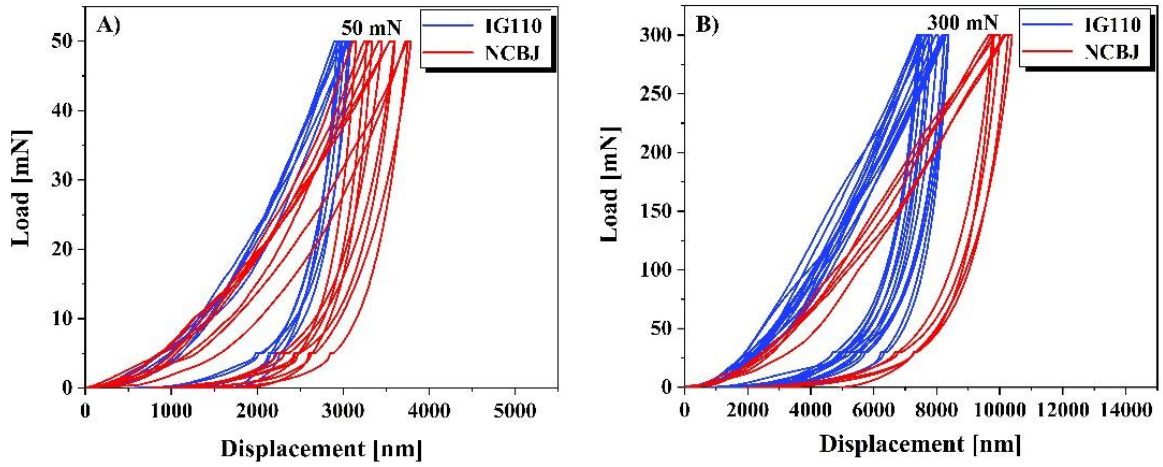

Fig. 3. Load-displacement curves recorded on nuclear graphite's IG-110 and NCBJ at A) 50 mN and B) 300 mN load.

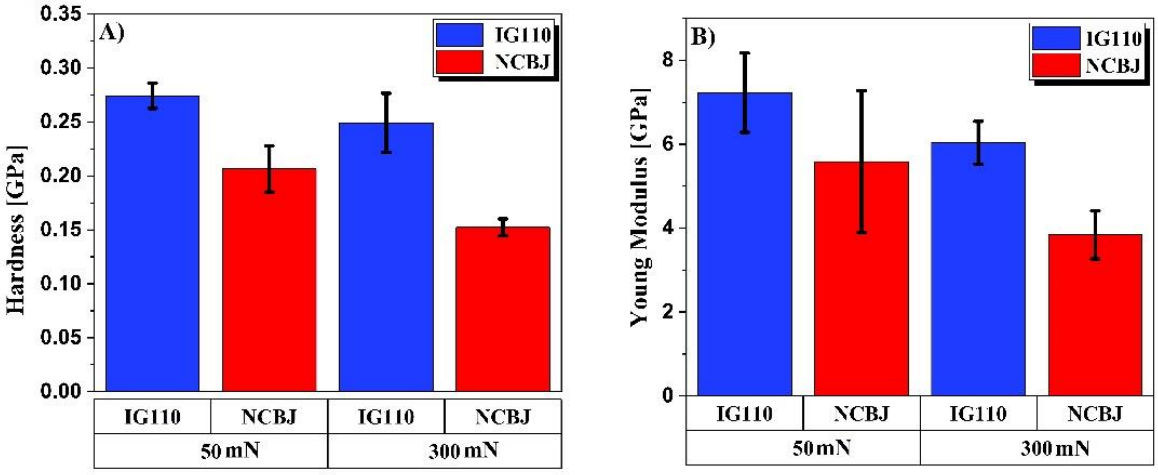

Fig. 4. A) Hardness and B) Young modulus of nuclear graphites IG-110 and NCBJ measured under 50 and 300 mN loads.

Generally speaking, all measurement methods showed the differences between IG-110 and NCBJ nuclear graphites. The microstructural analyses revealed bigger amount of discontinuities and large pores in the NCBJ graphite. These features seem to be evenly distributed in the whole volume of the material. Raman spectroscopy showed the presence of second order D-type bands which are related to defects. X-ray diffraction also pointed similar differences and suggests (similarly to Raman spectroscopy method) a turbostratic structure of the material. Finally, nanomechanical investigation showed scattering of the results which is related to discontinuities in the structure. It is expected that reported changes are related to the manufacturing method. IG-110 is one of the most commonly used graphite nowadays. Since its production method is stable, and expected structural and mechanical properties are predictable, this material is planned to be used in the next generation of nuclear reactors (e.g. HTR or MSR). NCBJ graphite is a material which was used in the decommissioned EWA research reactor at NCBJ and it is characterized by lower mechanical and probably structural properties, in comparison to IG-110. One should keep in mind that the samples tested in this work were not submitted to irradiation, hence their behavior might be different (especially at high dpa).
The presented work is part of a bigger project aiming to restore competences in testing materials dedicated to HTR technology. It is expected that it will be continued in the future. Especially important will be to investigate the impact of radiation damage and structure of the materials using TEM (Transmission Electron Microscopy) and Raman spectroscopy technique. Some nanomechanical tests on ion irradiated specimens are also planned. Both materials will be submitted to a 150 keV Ar and He ion irradiation process in the fluency range from 1x10^12 ions/cm2 to 2x10^17 ions/cm2. The link between different origins of the damage build up, especially from the structural point of view, will then be presented.

Conclusions

In this work, structural and mechanical properties of two different nuclear graphite materials (IG-110 and NCBJ) were examined by using Scanning Electron Microscopy, Raman Spectroscopy, X-ray Diffraction analysis and nanoindentation technique. The obtained results agree quantitatively, and qualitatively with the available literature data, pointing to the conclusion that the implemented testing

Pre-print version

methodology is correct. Both Raman analysis and X-ray diffraction techniques suggest turbostratic structure of the materials. All structural methods show discontinuities in the structure of the materials. This is supported by mechanical results and shows a possibility of correlating structural and mechanical properties. Finally, it has been shown that the IG-110 graphite is characterized by a more uniform structure than the NCBJ one.

Both structural and mechanical properties are highly dependent on the manufacturing techniques, therefore, the presented methodology can be used to verify their functional properties prior to material usage in the installation. Finally, the obtained results show that it will be possible to perform similar tests on the ion irradiated samples, and estimate the impact of radiation defects on the properties of nuclear graphites.

Acknowledgments

This work is one portion of the studies in the strategic Polish program of scientific research and development work "Social and economic development of Poland in the conditions of globalizing markets GOSPOSTRATEG" part of "Preparation of legal, organizational and technical instruments for the HTR implementation" financed by the National Centre for Research and Development (NCBiR) in Poland.

References:

1. G.E. Bacon, B.E. Warren, Acta Cryst., 9 (1956) 1029
2. W. Bollmann, J. Appl. Phys., 32 (1961) 869
3. J. Eapen, R. Krishna, T.D. Burchell, K.L. Murty, Mater. Res. Lett., 2 (2014) 43
4. J.A. Vreeling, O. Wouters, J.G. van der Laan, J. Nucl. Mater., 381 (2008) 68
5. Q. Huang, J. Li, R. Liu, L. Yan, H. Huang, J. Nucl. Mater., 491 (2017) 213
6. G. Zheng, P. Xu, K. Sridharan, T. Allen, J. Nucl. Mater., 446 (2014) 193
7. W-H. Huang, S-Ch. Tsai, C-W. Yang, J-J. Kai, J. Nucl. Mater. 254 (2014) 149
8. Z. Zhou, W.G. Bouwman, H. Schut, T.O. van Staveren, M.C.R. Heijna, C. Pappas, J. Nucl. Mater., 487 (2017) 323
9. R. Krishna, A.N. Jones, L. McDermott, B.J. Marsden, J. Nucl. Mater., 467 (2015) 557
10. T. Oku, A. Kurumada, Y. Imamura, M. Ishihara, J. Nucl. Mater., 381 (2008) 92
11. Z. He, P. Lian, J. Song, D. Zhang, Z. Liu, Q. Guo, J. Nucl. Mater., 511 (2018) 318
12. B.T. Kelly, Carbon, 20 (1982) 3
13. R. Krishna, A.N. Jones, B.J. Marsden, Rad. Phys. Chem. 107 (2015) 121
14. M.I. Heggie, I. Suarez-Martinez, C. Davidson, G. Haffenden, J. Nucl. Mater., 413 (2011) 150
15. E. Asari, Carbon 38 (2000) 1857
16. K. Niwase, Mater. Sci. Eng. A. Struct. 400-401 (2005) 101
17. N. Galy, N. Toulhoat, N. Moncoffre, Y. Pipon, N. Bererd, M.R. Ammar, P. Simon, D. Deldicque, P. Sainnsot, J. Nucl. Mater., 502 (2018) 20
18. J.E. Brocklehurst, B.T. Kelly, Carbon 31 (1993) 155
19. H. Wu, R. Gakhar, A. Chen, S. Lam, C.P. Marshall, R.O. Scarlat, J. Nucl. Mater., 528 (2020) 151802
20. A. J.J. Jasinski, L. Kurpaska, M. Lubas, M. Lesniak, J. Jasinski, M. Sitarz, Journal of Molecular Structure 1126 (2016) 165
21. B. M. Lubas, M. Sitarz, J.J. Jasinski, P. Jelen, L. Klita, P. Podsiad, J. Jasinski, Spectrochimica Acta Part A: Molecular and Biomolecular Spectroscopy 133 (2014) 883

Pre-print version

22. L.G. Cancado, K. Takai, T. Enoki, M. Endo, Y.a. Kim, H. Mizusaki, A. Jorio, L.N. Coelho, R. Magalha˜es-Paniago, M.a. Pimenta, Appl. Phys. Lett. 88 (16) (2006) 163106
23. M. a Pimenta, G. Dresselhaus, M.S. Dresselhaus, L.G. Cançado, a. Jorio, R. Saito, Phys. Chem. Chem. Phys. 9 (11) (2007) 1276
24. C. Olivier, G.M. Pharr, J. Mater. Res. 7 (1992) 1564
25. J.R. Cost, K.R. Janowski, R.C. Rossi, The Philosophical Magazine: A Journal of Theoretical Experimental and Applied Physics 17 (2006) 851
26. H. Kakui, T. Oku, J. Nucl. Mater., 137 (1986) 124
27. F. Tuinstra and J. L. Koenig, J. Phys. Chem., 1970, 53, 1126.
28. F. Tuinstra and J. L. Koenig, J. Compos. Mater., 4 (1970) 492
29. M. A. Pimenta, G. Dresselhaus, M. S. Dresselhaus, L. G. Cançado, A. Jorio and R. Saito, Phys. Chem. Chem. Phys., 9 (2007) 1276
30. M. Gawęda, P. Jeleń, E. Długoń, A. Wajda, M. Leśniak, W. Simka, M. Sowa, R. Detsch, A.R. Boccaccini, M. Sitarz J. Am. Ceram. Soc., 101 (2018) 590
31. M. Bik, M. Stygar, P. Jeleń, J. Dąbrowa, M. Leśniak, T. Brylewski, M. Sitarz, Int. J. Hydrog. Energy 42 (2017) 27298
32. M. Dudek, B. Adamczyk, M. Sitarz, M. Śliwa, R. Lach, M. Skrzypkiewicz, A. Raźniak, M, Ziąbka, J. Zuwała, P, Grzywacz, Biomass and Bioenergy 119 (2018) 144
33. M.S. Seehra, A.S. Pavlovic et al., Carbon 31 (1993) 557
34. O.A. Maslova, M.R. Ammar, et al., Phys. Rev. B Condens. Matter Mater. Phys. 86 (13) (2012) 1
35. A.C. Ferrari, J.C. Meyer, et al., Phys. Rev. Lett. 97 (18) (2006) 1

Link the the published version of the manuscript:
https://doi.org/10.1016/j.molstruc.2020.128370

Pre-print version